Synthesis, structure and oxygen-storage capacity of $Pr_{1-x}Zr_xO_{2-\delta}$ and $Pr_{1-x-y}Pd_yZr_xO_{2-\delta}$

Manjunath B. Bellakki [a], C. Shivakumara [a], Tinku Baidya [a],
A.S. Prakash [b], N.Y. Vasanthacharya [a], M.S. Hegde [a],*

[a] Solid State and Structural Chemistry Unit, Indian Institute of Science, Bangalore 560012, India
[b] Functional Materials Division Central Electrochemical Research Institute, Karaikudi 630006, Tamil Nadu, India

Abstract

Nanocrystalline $Pr_{1-x}Zr_xO_{2-\delta}$ ($0 \leq x \leq 1$) and $Pr_{1-x-y}Pd_yZr_xO_{2-\delta}$ ($x = 0.50$, $y = 0.02$) solid solutions have been synthesized by a single step solution combustion method. The whole range of solid solution compositions crystallize in cubic fluorite structure. The lattice parameter 'a' linearly varied up to $x = 1.0$. Oxygen-storage capacity (OSC) and redox properties of $Pr_{1-x}Zr_xO_{2-\delta}$ ($0.0 \leq x \leq 0.8$) solid solutions have been investigated by temperature-programmed reduction (TPR) and are compared with those of $Ce_{1-x}Zr_xO_2$. $Pr_{1-x}Zr_xO_{2-\delta}$ exhibited H_2 uptake and CO oxidation at a lower temperature than $Ce_{1-x}Zr_xO_2$. Small amount of Pd ion ($y = 0.02$) substitution was found to bring down the temperature of oxygen release–storage significantly.
© 2007 Elsevier Ltd. All rights reserved.

Keywords: A. Oxides; B. Chemical synthesis; C. X-ray diffraction; D. Catalytic properties

1. Introduction

The solid solutions of ceria with zirconia, $Ce_{1-x}Zr_xO_2$ are a well known oxygen storage material for exhaust catalysis. The unique feature of oxygen storage material is to release or store oxygen under fuel rich and fuel lean conditions, respectively. The loosely bound lattice oxygen of $Ce_{1-x}Zr_xO_2$ would oxidize either CO or C_nH_y (hydrocarbons) and the vacant oxide ion sites created would be filled by the stream oxygen under fuel lean conditions:

$$Ce_{0.7}Zr_{0.3}O_2 + \delta CO \rightarrow Ce_{0.7}Zr_{0.3}O_{2-\delta} + \delta CO_2$$

$$Ce_{0.7}Zr_{0.3}O_{2-\delta} + \tfrac{\delta}{2}O_2 \rightarrow Ce_{0.7}Zr_{0.3}O_2$$
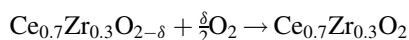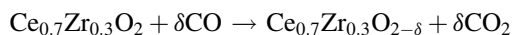
Reversible deintercalation–intercalation of oxygen to the extent of δ is defined as the oxygen storage capacity, OSC [1]. For pure CeO_2, δ is ~0.01 and for $Ce_{0.7}Zr_{0.3}O_2$, δ is ~ 0.2. ZrO_2 cannot be reduced by H_2 or CO whereas Ce^{4+} ion can be reduced to Ce^{3+} in the $Ce_{1-x}Zr_xO_2$ solid solution at a lower temperature (<500 °C) and to a large extent. The reason for such a behavior is due to destabilization of oxygen sublattice of the fluorite structure of $Ce_{1-x}Zr_xO_2$. Coordination of both Ce^{4+} and Zr^{4+} in the ideal fluorite is 8 but in the solid solution, both Ce and Zr ions have 4 + 4

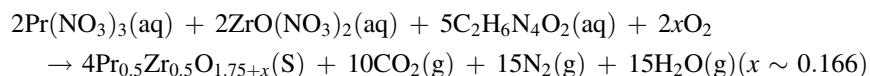
coordination leading to four Zr(Ce)–O short and four Zr(Ce)–O long bands. The four Ce–O bonds in $Ce_{1-x}Zr_xO_2$ are longer than the Ce–O bonds in CeO_2 and hence they can be reduced more easily [2,3].

Pr is the next element in the lanthanide series and Pr_6O_{11} is its most stable oxide. Extensive studies have been done by Eyring on the defect fluorite structure of Pr_nO_{2n-2} [4]. Pr_6O_{11} crystallizes in defect fluorite structure. Pr_6O_{11} can be more easily reduced to Pr_2O_3 than CeO_2 to Ce_2O_3. Hence, $Pr_{1-x}Zr_xO_{2-\delta}$ solid solutions are expected to be a better oxygen storage material. There are a few reports in the literature on the synthesis, structure and properties of PrO_y–ZrO_2 solid solution. Narula et al. have studied solid solutions of CeO_2–ZrO_2, PrO_y–CeO_2 and PrO_y–ZrO_2 and the compounds were synthesized by sol–gel method. The synthesized materials were calcined up to 900 °C to obtain crystalline phases and it resulted in low oxygen-storage capacity [5]. PrO_y–ZrO_2 with Pr upto 15% is shown to crystallize in tetragonal ZrO_2 structure and study was aimed at stabilizing tetragonal ZrO_2 by Pr ion [6]. PrO_y–ZrO_2 solid solution by hydroxide coprecipitation method has also been reported and is shown that Pr upto 17% could be substituted in ZrO_2 and these solid solutions crystallize in cubic fluorite structure [7]. Defect fluorite $Re_{0.6}Zr_{0.4-x}Y_xO_{2-\delta}$ (Re = Ce, Pr) have been reported to show high oxygen mobilities due to oxide ion defects induced by Pr and Y ion in $Pr_{0.6}Zr_{0.4-x}Y_xO_{2-\delta}$ [8]. However, there is no report on the formation of complete solid solution of $Pr_{1-x}Zr_xO_{2-\delta}$ ($0 \leq x \leq 1$) and their structure and oxygen-storage capacity.

Here we report the synthesis of nano $Pr_{1-x}Zr_xO_{2-\delta}$ ($0 \leq x \leq 1$) solid solution by single step solution combustion method and their structure, oxygen-storage capacity from H_2/TPR and CO/TPR reactions. Further, oxygen-storage capacity is demonstrated by the oxidation of CO by the utilization of the lattice oxygen to form CO_2 and its replacement by O_2. Furthermore, we show that substitution of Pd ion in $Pr_{1-x}Zr_xO_{2-\delta}$ enhances OSC at a lower temperature.

2. Experimental

$Pr_{1-x}Zr_xO_{2-\delta}$ ($0 \leq x \leq 1$) solid solutions were prepared by taking stoichiometric amounts of praseodymium oxide (Pr_6O_{11} 99.99% Indian Rare Earths) dissolved in dilute nitric acid, zirconyl nitrate, $ZrO(NO_3)_2 \cdot 6H_2O$ (Aldrich) and oxalyl dihydrazide fuel (ODH, prepared by the reaction of 1 mol of diethyl oxalate and 2 mol of hydrazine hydrate). In a typical preparation of $Pr_{0.5}Zr_{0.5}O_{2-\delta}$, 4.89 mmoles of praseodymium oxide (Pr_6O_{11}), 29.40 mmoles of zirconyl nitrate (in solution) and 73.42 mmoles of ODH, were taken in a borosilicate dish of 130 cm³ capacity. The reactants were dissolved in 20 ml water and introduced into a preheated muffle furnace at 500 °C. The solution boiled with frothing, foaming and ignited to burn with a flame (~1000 °C) yielding a voluminous solid product. Similarly pure ZrO_2 and $PrO_{2-\delta}$ were also prepared by the combustion method taking $ZrO(NO_3)_2 \cdot 6H_2O$ or praseodymium oxide, respectively. The chemical reaction for the formation of a solid solution by a combustion process, for example $Pr_{0.5}Zr_{0.5}O_2$, is as follows:

$$2Pr(NO_3)_3(aq) + 2ZrO(NO_3)_2(aq) + 5C_2H_6N_4O_2(aq) + 2xO_2$$
$$\rightarrow 4Pr_{0.5}Zr_{0.5}O_{1.75+x}(S) + 10CO_2(g) + 15N_2(g) + 15H_2O(g)(x \sim 0.166)$$

$Pr_{0.48}Pd_{0.02}Zr_{0.5}O_{2-\delta}$ was synthesized by taking Pr_6O_{11}, $PdCl_2$, $ZrO(NO_3)_2$ (in solution) and ODH in the mole ratio of 0.48:0.02:0.5:1.22. In typical reaction, 4.89 mmoles of praseodymium oxide (Pr_6O_{11}), 30.58 mmoles of zirconyl nitrate (in solution), 1.223 mmoles of palladium chloride and 74.65 mmoles of ODH were used.

X-ray diffraction (XRD) patterns of all the oxides synthesized were recorded on a Philips X'Pert X-ray diffractometer with Cu Kα source (λ = 1.5418 Å) at a scan rate of 0.5 °/min with 0.02 step size in the 2θ range 10–80°. Rietveld refinement of the structures were carried out using Fullprof program.

Hydrogen uptake studies were carried out using a temperature-programmed reduction (TPR) system with 5% H_2/Ar. About 100 mg of sample in a granular form (40–80 mesh powder) was placed in a fixed bed tubular reactor, over which 5% H_2 in Ar was continuously passed at a heating rate of 10 °C min⁻¹. The volume of hydrogen uptake, calibrated against a known amount of CuO, was measured using a TCD detector.

To understand the activity of lattice oxygen, CO oxidation over these oxides in absence of feed oxygen was done in a temperature-programmed reaction system equipped with a quadrupole mass spectrometer SX200 (VG Scientific Ltd., England) for product analysis in a packed bed tubular quartz reactor (dimension 25 cm × 0.4 cm) at atmospheric pressure. Typically, 250 mg of the catalyst (40/80 mesh size) diluted with SiO_2 (30/60 mesh size) was loaded in the

reactor to get a column length of 2.2 cm and endings were plugged with ceramic wool. For all the reactions, the total flow was kept fixed at 100 sccm to achieve a gas hourly space velocity (GHSV) of 10,000 h^{-1}. Before the catalytic test, the as-prepared catalyst was heated in O_2 flow at 200 °C for 1 h followed by degassing in He flow to the experimental temperature. The reactions were carried out as a function of temperature with a linear heating rate of 10 °C min^{-1}.
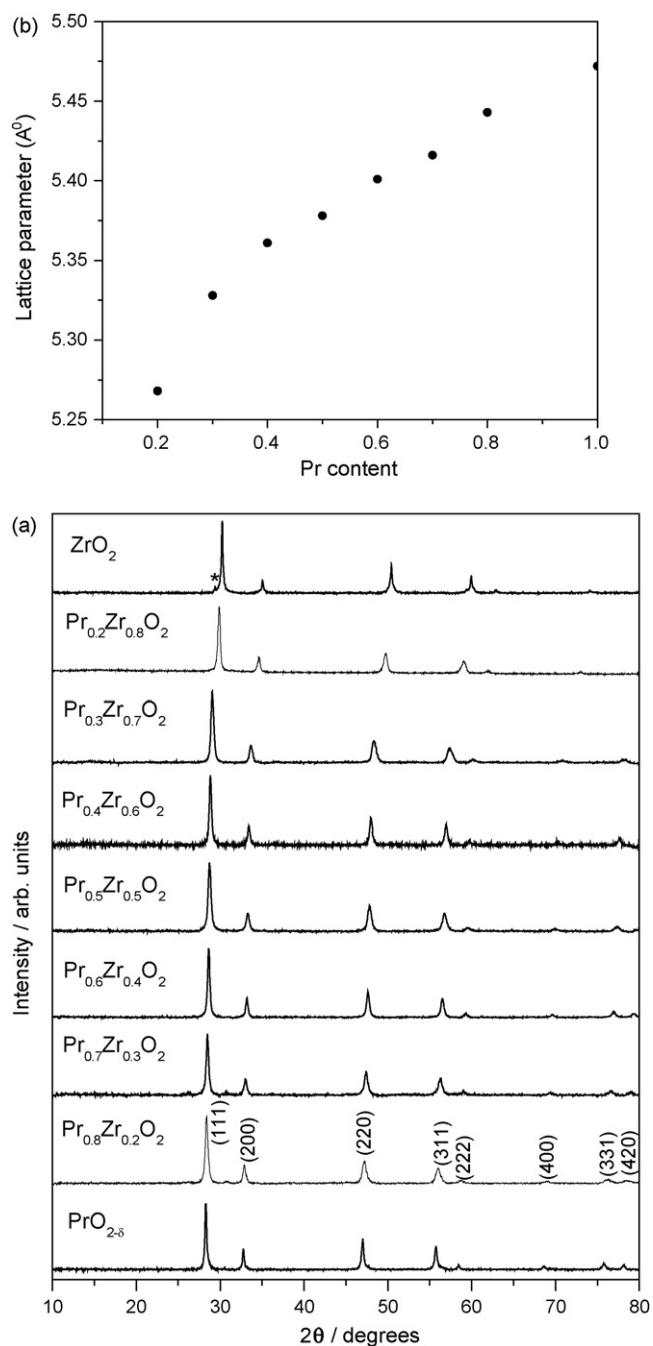

Fig. 1. (a) Powder XRD pattern of $Pr_{1-x}Zr_xO_{2-\delta}$ ($0 \leq x \leq 1$) (in ZrO_2, asterisk indicates monoclinic impurity phase). (b) Plot of lattice parameter 'a' vs. composition of Pr.

3. Results and discussion

Powder XRD pattern of $Pr_{1-x}Zr_xO_{2-\delta}$ ($0 \leq x \leq 1$) solid solutions are shown in Fig. 1a. The XRD patterns can be indexed to fluorite structure with space group $Fm3m$ (2 2 5). As can be seen from the figure, solid solution of $Pr_{1-x}Zr_xO_{2-\delta}$ is formed between PrO_y and ZrO_2 in the entire range $x = 0$–1. The structural parameters are refined by Rietveld method using Fullprof program. Typical refined XRD patterns of (a) $Pr_{0.5}Zr_{0.5}O_{2-\delta}$ and (b) $Pr_{0.4}Zr_{0.6}O_{2-\delta}$ compounds are given in Fig. 2. Oxygen content was fixed to the value obtained from the valencies of $Zr = +4$ and $Pr = +3.66$. In Table 1, we have summarized refined parameters. Lattice parameter and cell volume increases with increase in Pr content. Lattice parameter as a function of Pr content is given in Fig. 1(b). Oxygen estimation of $PrO_{2-\delta}$ was done by idiometric method and the composition is found to be $Pr_6O_{11\pm0.02}$. However, $Pr_{0.5}Zr_{0.5}O_{2-\delta}$ does not dissolve in HCl and so oxygen could not be estimated by idiometric titrations. In the $Pr_{1-x}Zr_xO_{2-\delta}$ solid solution, oxidation state of Pr is assumed to be same as in Pr_6O_{11} since the combustion synthesized Pr oxide also gave the composition Pr_6O_{11} (JCPDS No. 42-1121). Further, a plot of lattice parameter of $Pr_{1-x}Zr_xO_{2-\delta}$ versus composition of Pr was linear for $x = 0.3$–1 (Fig. 1b); $x = 1$ being Pr_6O_{11}. Therefore, oxidation state of Pr in the solid solution is the same as in Pr_6O_{11}. There are no literature values for lattice parameter for whole range of composition of $Pr_{1-x}Zr_xO_{2-\delta}$. This is the first study on the formation of complete solid solution of $Pr_{1-x}Zr_xO_{2-\delta}$ ($0 \leq x \leq 1$) and their structure and oxygen-storage capacity.
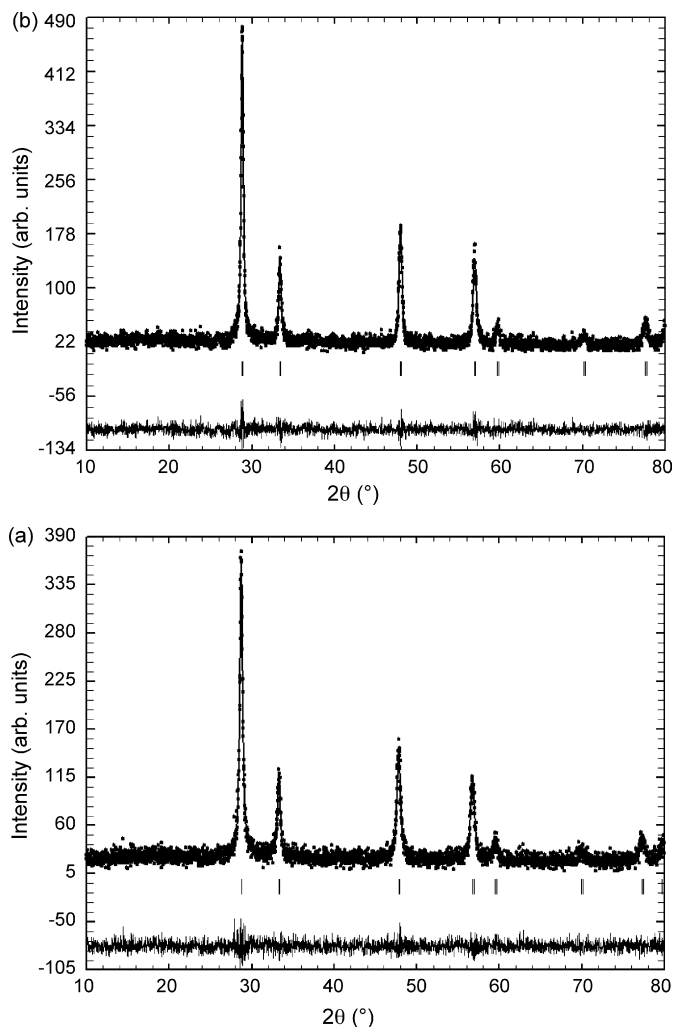

Fig. 2. Retvield refined XRD pattern of (a) $Pr_{0.5}Zr_{0.5}O_{1.916}$ and (b) $Pr_{0.4}Zr_{0.6}O_{1.933}$.

Table 1
Rietveld refined parameters and selected bond lengths for $Zr_{1-x}Pr_xO_{2-\delta}$ ($0 \leq x \leq 1$)

Compounds	Lattice parameter a (Å)	Cell volume (Å³)	R_f (%)	Bond distance Zr/Pr–O (Å)
ZrO_2	5.113(2)	134.102	5.129	2.214
$Pr_{0.2}Zr_{0.8}O_{1.966}$	5.199(1)	140.507	5.557	2.251
$Pr_{0.3}Zr_{0.7}O_{1.949}$	5.328(2)	151.325	5.273	2.307
$Pr_{0.4}Zr_{0.6}O_{1.933}$	5.361(1)	154.123	4.359	2.321
$Pr_{0.5}Zr_{0.5}O_{1.916}$	5.378(2)	155.552	5.099	2.328
$Pr_{0.6}Zr_{0.4}O_{1.899}$	5.401(1)	157.632	4.907	2.338
$Pr_{0.7}Zr_{0.3}O_{1.883}$	5.416(2)	158.902	6.757	2.345
$Pr_{0.8}Zr_{0.2}O_{1.866}$	5.419(1)	159.103	1.127	2.346
$PrO_{1.833}$	5.472(1)	163.851	5.115	2.369

Space group: *Fm-3m*; Zr/Pr (4a)-(0, 0, 0); O (8c)–(1/4, 1/4, 1/4).
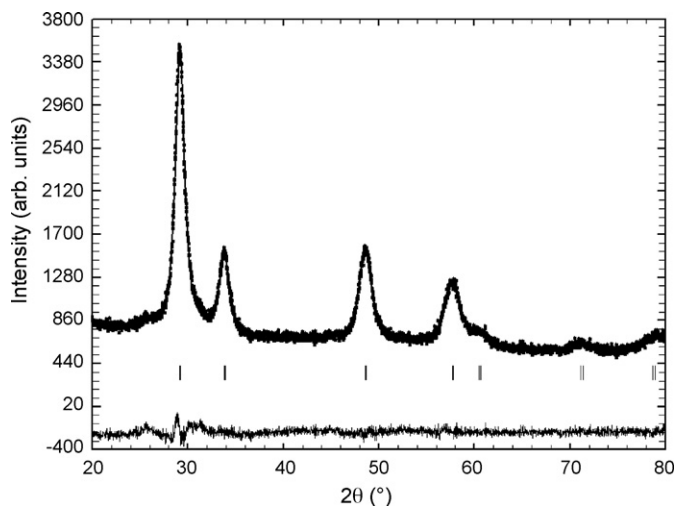
In Fig. 3, the Rietveld refined XRD pattern of $Pr_{0.48}Pd_{0.02}Zr_{0.5}O_{2-\delta}$, is shown. The profile fits well to fluorite structure. The lattice parameter 'a' is 5.297(2) Å which is lower than $Pr_{0.5}Zr_{0.5}O_{2-\delta}$ ($a = 5.378(2)$) indicating substitution of Pd ion in $Pr_{0.5}Zr_{0.5}O_{2-\delta}$. In the XRD of $Pr_{0.48}Pd_{0.02}Zr_{0.5}O_{2-\delta}$ ($\delta \sim 0.165$), diffraction lines due to Pd metal or PdO could not be detected.

Oxygen release/uptake of $Pr_{0.5}Zr_{0.5}O_{2-\delta}$ was investigated by TPR in both reduction and oxidation cycles and we characterized the reduction product of $Pr_{0.5}Zr_{0.5}O_{2-\delta}$ by XRD. As prepared $Pr_{0.5}Zr_{0.5}O_{2-\delta}$ is cubic fluorite with $a = 5.378(2)$ Å (Fig. 4a). The reduction of $Pr_{0.5}Zr_{0.5}O_{2-\delta}$ upto 800 °C in the TPR shows weak reflections due to a pyrochlore structure with lattice parameter, $a = 10.63$ Å (Fig. 4b) which is close to reported value of 10.71 Å [9]. Complete ordering of Pr^{3+}, Zr^{4+} ions does not seem to occur and hence the pyrochlore lines are weak. On reoxidation in air, the reduced yellowish white compound turns back to brown colour and the structure is restored to cubic fluorite (Fig. 4c).

Transmission electron microscopy image of typical $Pr_{0.5}Zr_{0.5}O_{2-\delta}$ is shown in Fig. 5(a). The average particle sizes are in the range of 25–30 nm. The corresponding electron diffraction pattern shown in Fig. 5(b) is composed of dark diffraction rings, indexed to fluorite structure.

3.1. Hydrogen uptake studies

Fig. 6(a–e) shows the H_2-TPR profile of $Pr_{1-x}Zr_xO_{2-\delta}$ ($0 \leq x \leq 0.8$). TPR profile of $Ce_{0.5}Zr_{0.5}O_2$ (Fig. 6f) is given for comparison. Notice the Y scales are different in the plots for different compositions. Total reduction from 30 to 800 °C has been carried out for all the compositions. Total hydrogen uptake is obtained from the integrated values

Fig. 3. Retvield refined XRD pattern of $Pr_{0.48}Pd_{0.02}Zr_{0.5}O_{1.898}$.
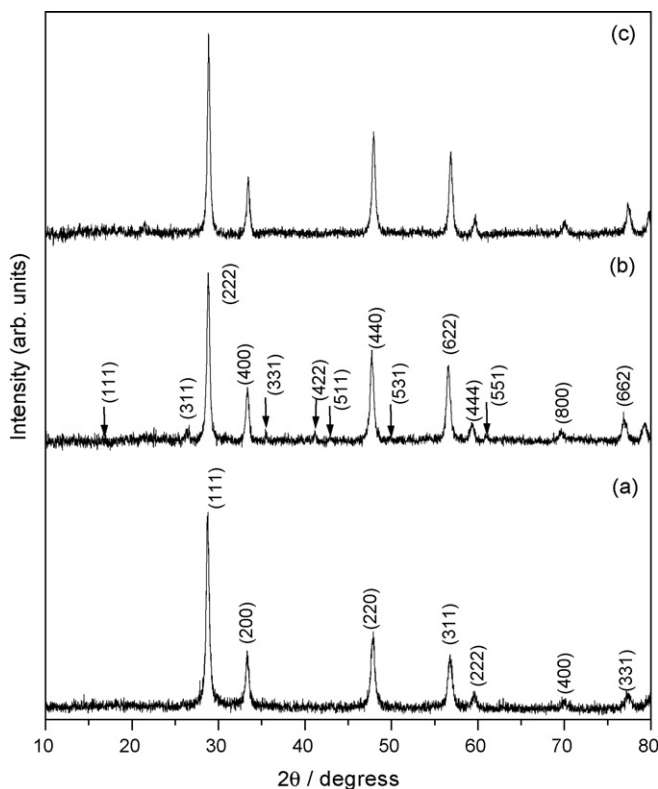
Fig. 4. Powder XRD pattern of (a) $Pr_{0.5}Zr_{0.5}O_{1.916}$, (b) reduced product of $Pr_{0.5}Zr_{0.5}O_{1.916}$ (pyrochlore structure) and (c) oxidized product of pyrochlore structure (b).

from 30 to 800 °C and they are given in Table 2. As can be seen from the curve (a) of Fig. 6, Pr_6O_{11} gets reduced below 550 °C and the volume of H_2 uptake corresponds to reduction of Pr_6O_{11} to Pr_2O_3. Indeed, light green Pr_2O_3 is formed. Contrary to this, only the surface oxygen can be removed from CeO_2 between ∼400 and 500 °C and complete reduction does not occur below 550 °C. As the Zr substitution is increased from 20 to 80% in Pr_6O_{11}, H_2 uptake profiles give reduction peaks, one at lower temperature ∼350 °C and the other at higher temperature ∼650 °C. Compositions of the reduced oxides derived from the total oxygen removed upto 800 °C are summarized in Table 2. OSC measured from the H_2 uptake study shows that Pr ion gets reduced to +3 state and the resulting reduced oxide was

Table 2
Integrated TPR results; comparison of oxygen-storage capacities of $Zr_{1-x}Pr_xO_{2-\delta}$ ($0 \leq x \leq 1$) with the reported values

| Sample	Composition after H_2 uptake	OSC μm/g (30–800 °C)	OSC μm/g (30–900 °C)[a]
$Pr_{0.2}Zr_{0.8}O_{1.966}$	$Pr_{0.2}Zr_{0.8}O_{1.94}$	187	–
$Pr_{0.25}Zr_{0.75}O_{1.957}$	–	–	185
$Pr_{0.3}Zr_{0.7}O_{1.949}$	$Pr_{0.3}Zr_{0.7}O_{1.85}$	705	–
$Pr_{0.4}Zr_{0.6}O_{1.933}$	$Pr_{0.4}Zr_{0.6}O_{1.82}$	781	–
$Pr_{0.5}Zr_{0.5}O_{1.916}$	$Pr_{0.5}Zr_{0.5}O_{1.73}$	1254	597
$Pr_{0.6}Zr_{0.4}O_{1.899}$	$Pr_{0.6}Zr_{0.4}O_{1.78}$	1116	1430
$Pr_{0.7}Zr_{0.3}O_{1.883}$	$Pr_{0.7}Zr_{0.3}O_{1.68}$	1312	–
$Pr_{0.75}Zr_{0.25}O_{1.873}$	–	–	978
$Pr_{0.8}Zr_{0.2}O_{1.866}$	$Pr_{0.8}Zr_{0.2}O_{1.62}$	1544	–
$PrO_{1.833}$	$PrO_{1.53}$	1777	1387
$Pr_{0.48}Pd_{0.02}Zr_{0.5}O_{1.899}$	$Pr_{0.48}Pd_{0.02}Zr_{0.5}O_{1.73}$	1141	–

[a] From Refs. [5] and [8].
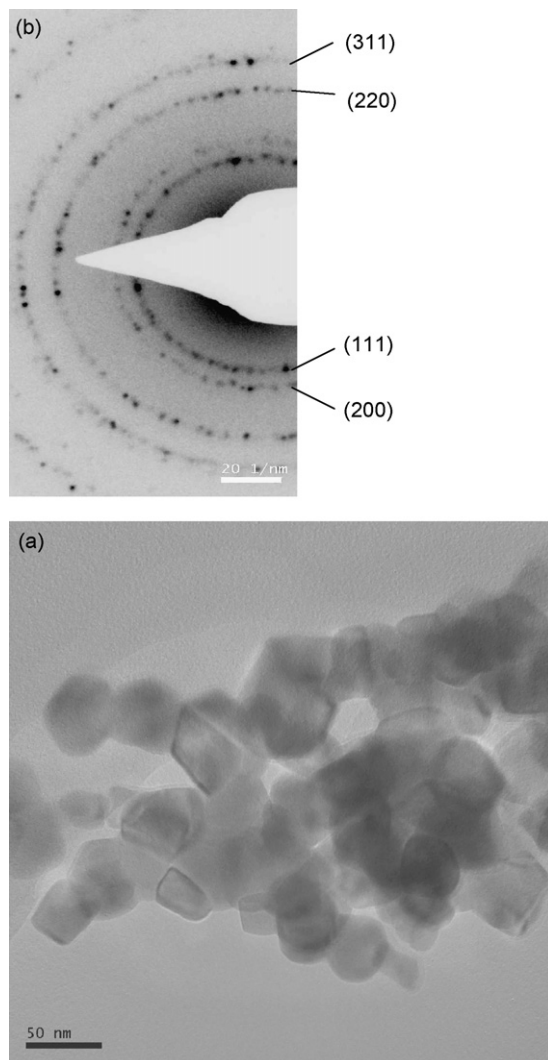
Fig. 5. (a) Transmission electron microscopy image and (b) the corresponding electron diffraction pattern of $Pr_{0.5}Zr_{0.5}O_{1.916}$.

pale green. For example, $Pr_{0.5}Zr_{0.5}O_{1.916}$ is reduced to $Pr_{0.5}Zr_{0.5}O_{1.73}$ where the entire Pr ion is reduced to Pr^{3+} state (see curve (c)). $Ce_{0.5}Zr_{0.5}O_2$ is reduced to $Ce_{0.5}Zr_{0.5}O_{1.75}$ in the H_2-TPR upto 800 °C (see curve (f) of Fig. 6), but the temperature at which major peaks obtained is at $\sim$500 °C. $Pr_{0.5}Zr_{0.5}O_{2-\delta}$ gets reduced at a lower temperature than $Ce_{0.5}Zr_{0.5}O_2$. Thus, the oxide ion is more labile in $Pr_{1-x}Zr_xO_{2-\delta}$ compared to $Ce_{0.5}Zr_{0.5}O_2$. OSC as measured from the H_2 uptake increases with Pr content (see Table 2). We have compared the total OSC from integrated H_2/TPR of $Pr_{1-x}Zr_xO_{2-\delta}$ with the values reported by Narula et al. [5]. They have reported OSC values from the integrated H_2/TPR upto 900 °C and our values are upto 800 °C. The OSC values are generally higher than the reported values except for $Pr_{0.6}Zr_{0.4}O_{2-\delta}$ composition.

With 2 at% Pd substitution, the temperature of reduction is decreased significantly (100–200 °C) (see curve (g) of Fig. 6). PdO itself gets reduced at around $\sim$45 °C and so the first reduction peak is not due to PdO reduction. The other two peaks at 350 and 575 °C are due to the reduction of Pr ion. The H/Pd molar ratio obtained from the first peak is 6.5. If the first peak is due to Pd^{2+} ion reduction to Pd^0, H/Pd ratio should have been 2 due to $PdO + H_2 \rightarrow Pd + H_2O$. The higher H/Pd ratio observed here demonstrates that part of Pr ion also gets reduced at a temperature much below Pr_6O_{11} or Pr ion in the $Pr_{0.5}Zr_{0.5}O_{1.916}$. The second and the third peak of the H_2 uptake can be attributed to the reduction of bulk $Pr^{3.66+}$ ion which also occurs at lower temperature than the Pr ion in ZrO_2.
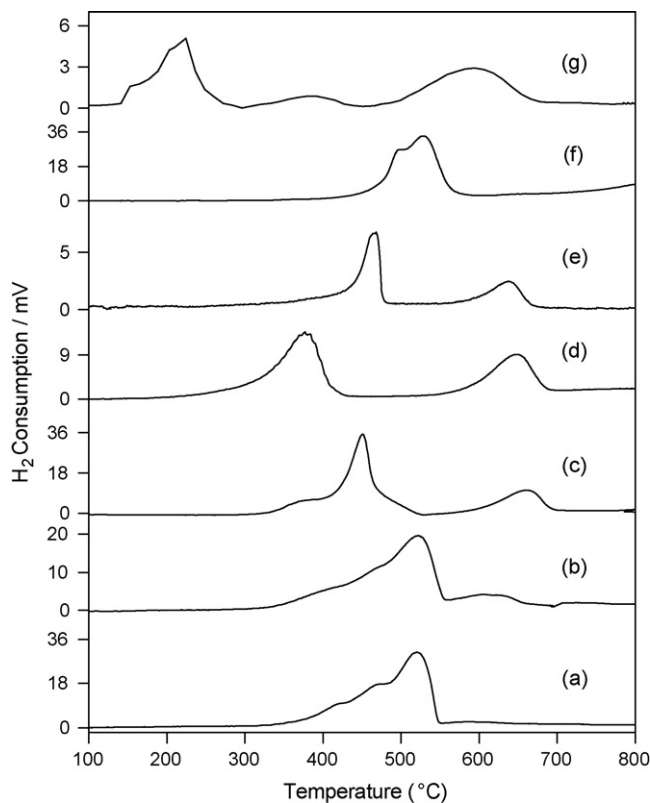
Fig. 6. TPR profiles of pure Pr_6O_{11} (curve a), $Pr_{1-x}Zr_xO_{2-\delta}$ (x = 0.3, 0.5, 0.6 and 0.8) (curves b–e) solid solutions, and $Ce_{0.5}Zr_{0.5}O_2$ (curve f), ($Pr_{0.48}Pd_{0.02}Zr_{0.5}O_{1.899}$) (curve g). Notice difference in Y scale for different samples.

3.2. CO oxidation study

To understand the reactivity of lattice oxygen, CO-TPR was carried out in absence of feed oxygen. Fig. 7(a) shows the CO oxidation profile over $Pr_{0.7}Zr_{0.3}O_{2-\delta}$, $Pr_{0.5}Zr_{0.5}O_{2-\delta}$, $Pr_{0.48}Pd_{0.02}Zr_{0.5}O_{2-\delta}$ and $Ce_{0.5}Zr_{0.5}O_{2-\delta}$ without feed oxygen. In Fig. 7(b) CO oxidation profile over $Pr_{0.7}Zr_{0.3}O_{2-\delta}$, $Pr_{0.3}Zr_{0.7}O_{2-\delta}$ and $PrO_{2-\delta}$ without feed oxygen are given. % CO conversion is a function of both temperature and Pr content in the $Pr_{1-x}Zr_xO_{2-\delta}$ solid solutions. The CO conversion begins in the following order: $Pr_{0.5}Zr_{0.5}O_{2-\delta}$ at 150 °C, $Pr_{0.7}Zr_{0.3}O_{2-\delta}$ at 250 °C and $Pr_{0.3}Zr_{0.7}O_{2-\delta}$ at 350 °C. The % CO conversion temperature is lowest at x = 0.5. However, final % CO conversion increases with the Pr content. The % CO conversion is ∼91% with $Pr_{0.7}Zr_{0.3}O_{2-\delta}$ and CO conversion over $PrO_{2-\delta}$ starts at ∼200 °C and maximum conversion is only 74% (see Fig. 7(b)). Thus, lability of oxygen is higher in $Pr_{1-x}Zr_xO_{2-\delta}$. After one cycle of CO/TPR in absence of oxygen, the compound gets reduced partially. The compound is oxidized by passing oxygen at 300 °C. Lattice oxygen utilized to form CO_2 is replenished and CO/TPR repeated in the second cycle as can be seen in the case of $Pr_{0.5}Zr_{0.5}O_{2-\delta}$.

With Pd ion substitution, at temperature as low as 100 °C, 20% CO conversion is observed and 80% conversion of CO occur below 250 °C. The catalyst regains oxygen upon O_2 passed over the catalyst at 250 °C and lattice oxygen can be utilized again. The Pd substituted compound is a true OSC material at much lower temperature than $Pr_{0.5}Zr_{0.5}O_{2-\delta}$. In the case of $Pr_{0.48}Pd_{0.02}Zr_{0.5}O_{2-\delta}$, CO oxidation starts at 50 °C. In our earlier studies, we have shown that Pt, Pd, or Rh ions substituted CeO_2 catalyst is far more reactive than the respective metal particles impregnated on CeO_2 [10–12]. We have also observed that substitution of noble metal ions in CeO_2, TiO_2, $Ce_{1-x}Ti_xO_2$, do not change the total reducibility of the support compared to the pure oxide except the decrease in the temperature of reduction. That CO adsorption occurs on Pt^{2+}, Pd^{2+} ions are shown by IR studies in our earlier paper [13]. The advantage of the presence of Pd ion in the support is to introduce a site for the adsorption of CO which is absent in the pure oxide. Hence, $Pr_{0.48}Pd_{0.02}Zr_{0.5}O_{2-\delta}$ shows much higher activity than $Pr_{0.5}Zr_{0.5}O_{2-\delta}$. Study of CO oxidation to CO_2 without stream
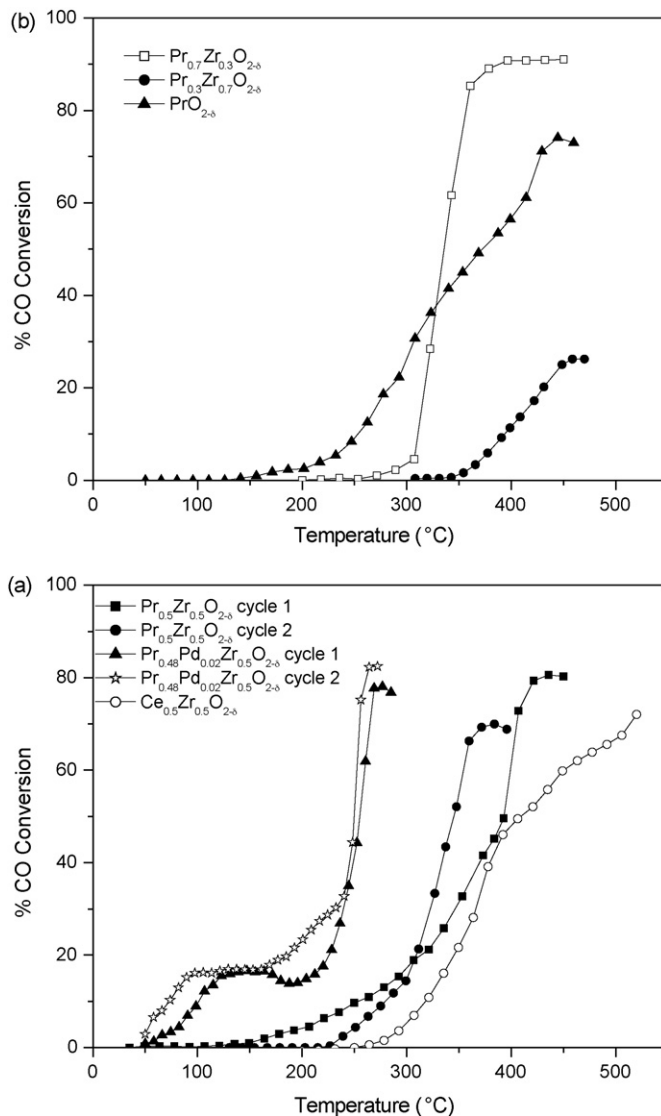
Fig. 7. % CO conversion as a function of temperature over (a) $Pr_{0.5}Zr_{0.5}O_{1.916}$, $Pr_{0.48}Pd_{0.02}Zr_{0.5}O_{1.898}$ and $Ce_{0.5}Zr_{0.5}O_2$ (b) $Pr_{0.3}Zr_{0.7}O_{1.494}$, $Pr_{0.7}Zr_{0.3}O_{1.916}$ and $PrO_{1.833}$ oxides under the reaction condition: CO = 0.25 cm^3 min^{-1}; 250 mg cat; GSHV = 10,000 h^{-1}; ramp rate = 15 K min^{-1}.

oxygen (O_2) is to find the availability of lattice oxygen in the oxides at a lower temperature. Of course Pd^{2+} ion will be reduced under (reducing) CO atmosphere. But the Pd^0 gets reoxidized in O_2. Hence, the CO to CO_2 reaction repeated after replacing the oxygen as seen from Fig. 7(a).

4. Conclusion

We have shown that nano $Pr_{1-x}Zr_xO_{2-\delta}$ ($x = 0$–1) crystallizing in fluorite structure can be prepared by single step solution combustion method and H_2/TPR as well as CO/TPR occur at a lower temperature than $Ce_{1-x}Zr_xO_2$. Pd ion substitution in $Pr_{1-x}Zr_xO_{2-\delta}$ enhances OSC property.

Acknowledgement

References

[1] A. Trovarelli, Catalysis by Ceria and Related Materials, Imperial College Press, London, 2002, p. 103.
[2] G. Dutta, U.V. Waghmare, T. Baidya, M.S. Hegde, K.R. Priolkar, P.R. Sarode, Catal. Lett. 108 (2006) 165.
[3] G. Dutta, U.V. Waghmare, T. Baidya, M.S. Hegde, K.R. Priolkar, P.R. Sarode, Chem. Mater. 18 (2006) 3249.
[4] L. Eyring, in: O. Toft Sorensen (Ed.), Nonstoichiometric Oxides, Academic Press, London, 1981, p. 344.
[5] C.K. Narula, P. Haack, W. Chun, H.-W. Jen, G.W. Graham, J. Phys. Chem. B 103 (1999) 3634.
[6] M.C. Caracoche, J.A. Marinez, P.C. Rivas, A.M. Rodriguez, Chem. Mater. 16 (2004) 4319.
[7] Y.-Q. Yao, Y.-F. Ying, M.-F. Luo, Y.-J. Wang, J.-M. Ma, Mater. Lett. 61 (2007) 192.
[8] H. He, H.X. Dai, K.W. Wong, C.T. Au, Appl. Catal. A 251 (2003) 61.
[9] M.A. Subramanian, G. Aravamudan, G.V. Subba Rao, Proc. Solid State Chem. 15 (1983) 55.
[10] P. Bera, K.C. Patil, V. Jayaram, G.N. Subbanna, M.S. Hegde, J. Catal. 196 (2000) 293.
[11] P. Bera, K.R. Priolkar, A. Gayen, P.R. Sarode, M.S. Hegde, S. Emura, R. Kumashiro, V. Jayaram, G.N. Subbanna, Chem. Mater. 15 (2003) 2048.
[12] A. Gayen, K.R. Priolkar, P.R. Sarode, V. Jayaram, M.S. Hegde, G.N. Subbanna, S. Emura, Chem. Mater. 16 (2004) 2317.
[13] P. Bera, A. Gayen, M.S. Hegde, N.P. Nalla, L. Spadaro, F. Frusteri, F. Arena, J. Phys. Chem. B 107 (2003) 6122.